Clays and Clay Minerals, Vol. 40, No. 2, 129–144, 1992.

THE CRYSTAL STRUCTURE OF BANNISTERITE

PETER J. HEANEY[1] AND JEFFREY E. POST
Department of Mineral Sciences, Smithsonian Institution, Washington, D.C. 20560

HOWARD T. EVANS, JR.
U.S. Geological Survey, Reston, Virginia 22092

Abstract—The crystal structure of bannisterite, a modulated, mica-like mineral species, of general composition $Ca_{0.5}(K,Na)_{0.5}(Mn,Fe,Mg,Zn)_{10}(Si,Al)_{16}O_{38}(OH)_8 \cdot nH_2O$, has been solved and refined for specimens from Franklin Furnace, New Jersey (FF), and Broken Hill, Australia (BH). The crystals are monoclinic in space group $A2/a$, with (for FF) $a = 22.265(1)$ Å, $b = 16.368(1)$ Å, $c = 24.668(2)$ Å, $\beta = 94.285(5)°$; and (for BH) $a = 22.286(1)$ Å, $b = 16.386(1)$ Å, $c = 24.575(2)$ Å, $\beta = 94.355(7)°$; $Z = 8$. Refinement with anisotropic thermal factors reached $R_w = 0.034$ (FF) and 0.039 (BH). Like stilpnomelane and ganophyllite, bannisterite has a modified 2:1 trioctahedral layer structure in which some of the tetrahedra are inverted towards the interlayer region and linked to inverted tetrahedra in the opposite layer. The octahedral sheet is strongly corrugated along *b*. The tetrahedral sheet consists of 5-, 6-, and 7-fold rings, and bond distance calculations indicate that Al is concentrated into two of the four inverted tetrahedra. The interlayer Ca, K, and H_2O species are highly disordered, as indicated by anomalously large temperature factors and partial occupancies. Localized differences in the Al/Si arrangements in the inverted tetrahedra induce disorder among the interlayer cations.

Key Words—Bannisterite, Interlayer cations, Layer structure, Modulated structure, X-ray structure refinement.

INTRODUCTION

Bannisterite, a modulated 2:1-type (mica-like) layer silicate from the Benallt mine in Caernarvonshire, Wales was first described and analyzed by Foshag (1936), but he incorrectly identified it as ganophyllite, a close structural relative. W. C. Smith (1948) compared the optical behavior exhibited by so-called ganophyllite specimens from the Benallt mine with that displayed by ganophyllite from the type locality at the Harstig mine in Pajsberg, Sweden. He suggested that two structurally distinct minerals had been grouped under one name. Single crystal X-ray precession experiments by M. L. Smith and Frondel (1968) confirmed W. C. Smith's surmise, and they gave the material from the Benallt mine the name bannisterite.

Bannisterite seems to occur relatively rarely, but important localities include Franklin Furnace, New Jersey (Smith and Frondel, 1968), Broken Hill, Australia (Plimer, 1977), Toba City, Japan (Matsubara and Kato, 1989), and Nyberget, Sweden (Ferrow et al., 1990), in addition to Caernarvonshire, Wales. At Franklin Furnace bannisterite is found as anhedral plates, sometimes measuring up to 5 cm in diameter, in association with a variety of other manganiferous minerals such as ganophyllite, axinite and rhodonite. Its color ranges from light brown to black with a resinous luster. In thin section bannisterite is pleochroic from pale yellow to brown.

The late Ian Threadgold (1979) solved the crystal structure of "partially dehydrated" bannisterite from Broken Hill, Australia. Threadgold presented a general description of the structure in an abstract, but his detailed solution has not been published. With the aid of Threadgold's abstract and some of his unpublished diagrams of portions of the bannisterite structure (S. W. Bailey, personal communication), we have solved the structures of two compositionally different bannisterite specimens from Broken Hill, Australia, and Franklin Furnace, New Jersey.

The present study in large part confirms Threadgold's model for the framework of this unusual layer silicate. In addition, we have found in the interlayer material significant positional disorder beyond that mentioned for the partially dehydrated specimen examined by Threadgold. Both crystals used in our study were in their natural, hydrated state. With the possible exception of zussmanite (see below), bannisterite is the first modulated structure determination at high resolution, allowing for detailed investigation into its crystal chemistry.

STRUCTURE DETERMINATION

Single crystals of bannisterite were selected from samples from Franklin Furnace, New Jersey (USNM No. C6253) and from Broken Hill, Australia (USNM No. 142892). Compositional analyses of these speci-

[1] Present address: Department of Geology and Geophysical Sciences, Princeton University, Princeton, New Jersey 08544.

Table 1. Compositions and formulas of bannisterite specimens studied. Data in weight percent from Dunn *et al.* (1981).

	Franklin, New Jersey[1] (USNM No. C6253)	Broken Hill, Australia[2] (USNM No. 142892)
SiO_2	46.6	45.8
Al_2O_3	3.9	4.0
Fe_2O_3	0.77	not deter.
FeO	5.60	17.4
MgO	3.1	0.3
CaO	1.2	1.5
MnO	23.7	20.8
ZnO	4.4	0.3
K_2O	1.10	0.65
Na_2O	0.08	0.25
H_2O^+	5.80	4.90
H_2O^-	3.37	3.82
Total	99.6	99.7

[1] Franklin Furnace, New Jersey: $Ca_{0.40}(K_{0.44}Na_{0.05})_{\Sigma 0.49}(Mn_{6.22}Fe_{1.45}Mg_{1.43}Zn_{1.01})_{\Sigma 10.11}(Si_{14.42}Al_{1.43}Fe_{0.18})_{\Sigma 16.03}O_{38}(OH)_8 \cdot 5.5H_2O$.

[2] Broken Hill, Australia: $Ca_{0.50}(K_{0.26}Na_{0.15})_{\Sigma 0.41}(Mn_{5.53}Fe_{4.57}Mg_{0.14}Zn_{0.07})_{\Sigma 10.31}(Si_{14.38}Al_{1.48})_{\Sigma 15.86}O_{38}(OH)_8 \cdot 5.1H_2O$.

mens have been reported by Dunn *et al.* (1981) and are reprinted in Table 1. When these analyses are renormalized to 38 oxygen atoms and 8 hydroxyl groups the formulas for the two samples are those given in Table 1. E. A. Ferrow (personal communication) determined that hydroxyl contents in bannisterite are not strictly stoichiometric, and therefore these formulas are approximate. The primary compositional difference between the two samples used in this study can be represented by the exchange of Fe ↔ (Mn,Mg,Zn) in octahedral coordination, with the sample from Broken Hill the more iron-rich of the two.

The crystals measured approximately 0.25 × 0.14 × 0.09 mm (Franklin Furnace), and 0.20 × 0.15 × 0.08 mm (Broken Hill). Precession, Weissenberg, and Laue photographs of both crystals revealed that bannisterite has an *A*-centered cell with an *a*-glide plane, and belongs to Laue class $2/m$. Inspection of the precession photographs produced by both bannisterite crystals suggests the presence of a prominent subcell characterized by $a' = a/4$, $b' = b/10$, and $c' = c$. This subcell corresponds to the pseudohexagonal pattern of the $(Mn,Fe)O_2$ octahedral layer (with $a'' = 6.54$ Å, $c'' = 24.67$ Å, $\gamma = 120.46°$), which dominates this structure and other modulated sheet silicates in this group. No indication of diffuse scattering was observed on any of these patterns.

Intensity data were collected by step-scans with a Krisel-automated Picker four-circle diffractometer fitted with a graphite monochrometer, using MoKα radiation. Data collection parameters are summarized in Table 2. Refinement of setting angles by the method of Hamilton (Ibers and Hamilton, 1974) for 20 reflections ($40° < 2\theta < 50°$) yielded similar sets of unit-cell parameters for the two crystals. These values are also listed in Table 2.

Table 2. Crystal and structure refinement data.

	Franklin	Broken Hill
Space group	*A2/a*	*A2/a*
Unit cell		
a (Å)	22.265(1)	22.286(1)
b (Å)	16.368(1)	16.386(1)
c (Å)	24.668(2)	24.575(2)
β (deg.)	94.285(5)	94.355(7)
V (Å^3)	8964.9(9)	8948.2(1.0)
20 range (deg.)	2–60	2–50
Data collected	*h, k,* ±*l*	±*h, k,* ±*l*
Stepscan parameters		
Step size (deg.)	0.025	0.025
Time/step (sec.)	2.0	2.0
Standard reflections	2	2
h, k, l	408, 0.10.0	408, 0.10.0
Time between standards (min.)	120	120
Merging *R* factor[1]	—	0.055
Unique reflections		
Observed	7117	6461
Unobserved	6024	2031
Parameters refined	774	778
R factors	0.039	0.034

[1] Calculated for observed and unobserved reflections.

Each reflection profile was examined graphically, and background limits were adjusted as needed. Absorption corrections were calculated for the Broken Hill bannisterite, using $\mu = 32.4$ cm^{-1}, with the Gaussian integration method in both the XTAL program (Stewart and Hall, 1988) and the program of Burnham (1963). The absorption corrections calculated by the two programs were virtually identical, and the transmission factors ranged from 0.45 to 0.75. Burnham's corrections were used for our working data sets, which also incorporated the usual Lorentz-polarization corrections, anomalous dispersion corrections, and in the last stages of refinement, an isotropic extinction correction.

An independent solution of the bannisterite structure was first attempted for the Broken Hill data set using the symbolic addition procedure for phase determination (Karle and Karle, 1966). The positions of the M atoms (Mn,Fe) and octahedral O atoms were immediately discernible in the *E*-maps and *F*(obs)-maps in the regions near $z = \frac{1}{4}$ and $\frac{3}{4}$. Well-resolved peaks representing the Si and O atoms adjacent to this sheet appeared, but the direct methods (using SIMPEL, MULTAN and hand methods) could not be made to reveal any information about the interlayer material, including the cross-linked silicate groups. Subsequently, a trial calculation was performed with structure factors for only the 12 Si atoms adjacent to the octahedral sheet as indicated by Threadgold (1979). The resultant electron density map revealed the 4 cross-linked atoms as suggested by Threadgold's projections, as well as the

10 octahedral cations. Least-squares refinement of 10 Fe and 16 Si atoms gave R_w (weighted reliability index) = 0.35. In the next electron density map the entire $M_{10}Si_{16}O_{38}(OH)_8$ framework structure emerged in sharp detail.

Refinement of the bannisterite structure then proceeded as follows: The $M_{10}Si_{16}O_{38}(OH)_8$ framework with M = Fe was treated in a block-matrix least-squares refinement, first using isotropic temperature factors, followed by a full anisotropic refinement, leading to $R_w = 0.071$. At this point only the atoms in the interlayer region remained to be located. On the basis of the electron-density peaks in the sections at $z = 0$ and ½ and the known compositions of the specimens, Ca and K(1) were placed on the 2-fold rotation axis (in 4*e*), and K(2) was positioned on an inversion center at the origin (in 4*a*). After further refinement with isotropic temperature factors, the observed Fourier maps showed that the images of Ca and K(2) were strongly elongated and nearly split in two. Accordingly, these atoms were removed to general positions with half occupancy. One water molecule with full occupancy [O(50)] and four water molecules with half occupancies [O(51)–O(54)] were introduced on density maxima, coordinated to the Ca atom at reasonable distances from the cation and from each other, as described in the following section. Further least-squares refinement showed these atoms to be stable, with moderately large thermal parameters and occupancies (allowed to vary) of approximately 50 percent. Successive difference maps indicated the locations of additional water molecules, creating a total of 11 water sites.

The final stages of refinement incorporated weights based on counting statistics ($1/\sigma$) and an isotropic extinction factor. All atoms were represented by anisotropic thermal ellipsoids, and variable occupancy factors for K and free water molecules. Unit occupancies were assumed for all framework atoms; occupancies were held at 0.5 for Ca, O(51), O(52), O(53), O(54), and unity for O(50). Water molecules O(55), O(56), and O(60) were located so as to avoid overlap with other atoms, and assigned 0.5 occupancy. The *F*(obs) map for Franklin Furnace showed a marked elongation of the peak for K(2), so this atom was displaced from the 2-fold axis to a general position. The final weighted reliability index for the Broken Hill structure is R_w = 0.039. An identical refinement [except for K(2)] for the Franklin Furnace structure yields 0.034. The corresponding goodness-of-fit factors are 2.66 and 4.29, respectively.

The final positional and occupational parameters and root-mean-square isotropic thermal displacements (estimated from $U_{ii}/3$) for the two structures are given in Table 3. The estimated standard deviations obtained in this way are probably 50 to 100 percent greater than those shown in Table 3, because of the neglect of cross terms in the least-squares analysis. Applying this correction (2x), the positional errors may be considered to be: for Fe(Mn), 0.0015 Å; for Si, 0.002 Å; for framework O, 0.005 Å. The uncertainties of the positions of the interlayer atoms, which have very large thermal eccentricities, are considerably larger.

Before the last stages of least-squares refinement an attempt was made to estimate the occupancies of the framework atoms, especially the octahedral M cations. Although the independent variation of occupancy parameters together with thermal parameters may ultimately become highly correlated, it was clear from these results that there is no significant ordering of Mg or Zn among any of the 10 octahedral sites (see Discussion, below). The microprobe analyses of Dunn *et al.* (1981) provide no analytical evidence for the presence of vacancies among the octahedral cations. Therefore, in the final refinement stages we have assumed full occupancy of the octahedral sites and completely random distribution of the 4 types of octahedral cations. Composite scattering factors for the octahedral cations were derived by combining those for Mn, Fe, Mg, and Zn in proportion to their analytical fractions (Table 1).

In a final *F*(obs) map calculated for the Broken Hill data with observed data less than $\sin\theta/\lambda = 0.4$, images of hydrogen atoms were sought for the hydroxyl groups in the octahedral layer [O(39)–O(46)] with only marginal success. Peaks were found opposite O(42), O(43), O(44), and O(46) at a distance of about 1.0 Å away from the octahedral sheet, but no positive density at all was found opposite the remaining 4 oxygen atoms. The observed peaks had maxima of about 0.6 $e/Å^3$, but were not clearly distinguished from prevalent noise maxima, which averaged about ± 0.06 $e/Å^3$, sometimes reaching ± 1.0 $e/Å^3$. While Threadgold (1979) showed the hydroxyl hydrogen atoms in his refinement of dehydrated bannisterite, we were unable to determine hydrogen positions from our refinements of hydrated bannisterites unequivocally.

All computations were carried out on a VAX780 and a SUN 4/110 workstation, using the XTAL86 program system (Stewart and Hall, 1988), except for the absorption corrections. Standard scattering factors for neutral atoms, anomalous dispersion parameters, and mass absorption coefficients were taken from Ibers and Hamilton (1974). Lists of observed anisotropic thermal parameters are given in Table 4. Calculated structure factors for the two structures are given in Tables 5 and 6. Tables 5 and 6 are available from the senior author on request.

DISCUSSION

Structure of the framework

Our determination of the general structure of the octahedral and tetrahedral framework of bannisterite is in good agreement with that described by Threadgold

https://doi.org/10.1346/CCMN.1992.0400201 Published online by Cambridge University Press

Table 3. Structure parameters for bannisterite. For each entry: first line is Broken Hill, second line is Franklin Furnace.

Atom	*x*	*y*	*z*	$\tilde{u}$, Å	Pop.
Octahedral cations:					
M(1)	0.06358(3)	0.39253(4)	0.25829(3)	0.119(2)	1.0
	0.06395(5)	0.39172(7)	0.25824(4)	0.097(3)	1.0
M(2)	0.06277(3)	0.19548(3)	0.24175(3)	0.109(2)	
	0.06248(5)	0.19552(6)	0.24150(4)	0.094(3)	
M(3)	0.18953(3)	0.48491(4)	0.25869(3)	0.120(2)	
	0.18958(5)	0.48451(6)	0.25857(4)	0.101(3)	
M(4)	0.18545(3)	0.28550(4)	0.24081(3)	0.119(2)	
	0.18614(5)	0.28580(7)	0.23989(4)	0.095(3)	
M(5)	0.18608(3)	0.08489(4)	0.23210(3)	0.128(2)	
	0.18593(5)	0.08659(6)	0.23173(4)	0.108(3)	
M(6)	0.31230(3)	0.38450(4)	0.24632(3)	0.126(2)	
	0.31203(5)	0.38372(6)	0.24574(4)	0.109(3)	
M(7)	0.31093(3)	0.18718(4)	0.23597(3)	0.121(2)	
	0.31049(5)	0.18732(6)	0.23522(4)	0.104(3)	
M(8)	0.43892(3)	0.49370(4)	0.26521(3)	0.140(2)	
	0.43868(5)	0.49424(6)	0.26580(4)	0.109(3)	
M(9)	0.43639(3)	0.29220(4)	0.24845(3)	0.111(2)	
	0.43620(5)	0.29186(6)	0.24771(4)	0.104(3)	
M(10)	0.43533(3)	0.09264(4)	0.23354(3)	0.124(2)	1.0
	0.43463(5)	0.09284(6)	0.23280(4)	0.108(3)	1.0
Tetrahedral cations:					
Si(1)	0.12276(6)	0.40089(7)	0.14051(6)	0.105(3)	1.0
	0.12270(8)	0.40077(11)	0.14081(7)	0.101(4)	1.0
Si(2)	0.39916(6)	0.40131(7)	0.14150(6)	0.106(3)	
	0.39940(8)	0.40175(11)	0.14188(7)	0.101(4)	
Si(3)	0.52154(6)	0.31697(7)	0.14636(5)	0.097(3)	
	0.52182(9)	0.31674(11)	0.14681(7)	0.099(4)	
Si(4)	0.52222(6)	0.13100(7)	0.12898(6)	0.103(3)	
	0.52240(9)	0.13016(11)	0.12889(7)	0.104(4)	
Si(5)	0.64427(6)	0.04517(7)	0.12842(6)	0.105(3)	
	0.64491(9)	0.04461(11)	0.12863(7)	0.103(4)	
Si(6)	0.63928(6)	0.41348(7)	0.15170(5)	0.094(3)	
	0.63959(9)	0.41334(11)	0.15176(7)	0.100(4)	
Si(7)	0.76188(6)	0.32840(7)	0.15216(5)	0.097(3)	
	0.76218(9)	0.32817(10)	0.15285(7)	0.100(4)	
Si(8)	0.76141(5)	0.14342(7)	0.14244(6)	0.102(3)	
	0.76175(9)	0.14303(10)	0.14316(7)	0.098(4)	
Si(9)	0.87505(6)	0.04534(7)	0.12707(6)	0.105(3)	
	0.87565(9)	0.04426(11)	0.12768(7)	0.102(4)	
Si(10)	0.88437(6)	0.41307(7)	0.15211(5)	0.098(3)	
	0.88471(8)	0.41233(11)	0.15251(7)	0.096(4)	
Si(11)	0.00105(6)	0.31627(7)	0.14439(6)	0.100(3)	
	0.00114(8)	0.31556(10)	0.14498(7)	0.096(4)	
Si(12)	−0.00225(6)	0.13038(7)	0.12698(6)	0.108(3)	
	−0.00145(9)	0.12907(11)	0.12746(7)	0.104(4)	
Si(13)	0.11169(6)	0.10688(7)	0.06476(6)	0.108(3)	
	0.11195(9)	0.10663(11)	0.06457(7)	0.109(4)	
Si(14)	0.18347(6)	0.27205(8)	0.06454(6)	0.096(3)	
	0.18290(9)	0.27325(11)	0.06420(7)	0.112(4)	
Si(15)	0.32627(6)	0.27292(8)	0.06505(6)	0.114(3)	
	0.32666(9)	0.27436(11)	0.06447(8)	0.115(4)	
Si(16)	0.39845(6)	0.10772(7)	0.06564(6)	0.106(3)	1.0
	0.39832(8)	0.10806(11)	0.06528(7)	0.103(4)	1.0
Framework oxygen atoms:					
O(1)	0.1384(2)	0.3901(2)	0.2052(2)	0.122(7)	1.0
	0.1376(2)	0.3892(3)	0.2052(2)	0.114(10)	1.0
O(2)	0.3959(2)	0.3922(2)	0.2063(1)	0.118(7)	
	0.3955(2)	0.3924(3)	0.2069(2)	0.111(10)	
O(3)	0.4793(2)	0.1914(2)	0.2884(1)	0.116(7)	
	0.4797(2)	0.1919(3)	0.2884(2)	0.114(10)	
O(4)	0.4808(2)	0.3903(2)	0.3072(1)	0.130(7)	
	0.4824(2)	0.3917(3)	0.3077(2)	0.122(10)	

Table 3. Continued.

Atom	*x*	*y*	*z*	$\tilde{u}$, Å	Pop.
O(5)	0.3564(2)	0.4791(2)	0.3075(2)	0.134(7)	
	0.3570(2)	0.4795(3)	0.3083(2)	0.128(10)	
O(6)	0.3564(2)	0.0850(2)	0.2826(2)	0.106(7)	
	0.3564(2)	0.0855(3)	0.2829(2)	0.107(10)	
O(7)	0.2319(2)	0.1794(2)	0.2820(2)	0.115(7)	
	0.2323(2)	0.1795(3)	0.2823(2)	0.106(10)	
O(8)	0.2317(2)	0.3730(2)	0.2930(1)	0.108(7)	
	0.2324(2)	0.3728(3)	0.2925(2)	0.108(10)	
O(9)	0.1134(2)	0.4773(2)	0.3089(2)	0.124(7)	
	0.1129(2)	0.4785(3)	0.3089(2)	0.120(10)	
O(10)	0.1071(2)	0.0870(2)	0.2818(2)	0.112(7)	
	0.1081(2)	0.0883(3)	0.2825(2)	0.108(10)	
O(11)	0.0129(2)	0.3061(2)	0.2094(2)	0.112(7)	
	0.0129(2)	0.3051(3)	0.2098(2)	0.112(10)	
O(12)	0.0127(2)	0.1098(2)	0.1910(2)	0.130(7)	
	0.0125(2)	0.1081(3)	0.1913(2)	0.115(10)	
O(13)	0.1033(2)	0.0975(2)	−0.0007(2)	0.149(7)	
	0.1029(2)	0.0964(3)	−0.0007(2)	0.154(9)	
O(14)	0.1670(2)	0.2985(2)	0.0001(2)	0.136(7)	
	0.1662(2)	0.3003(3)	0.0009(2)	0.142(10)	
O(15)	0.1303(2)	0.4967(2)	0.1257(2)	0.120(7)	
	0.1300(2)	0.4961(3)	0.1258(2)	0.127(10)	
O(16)	0.0537(2)	0.3726(2)	0.1221(2)	0.127(7)	
	0.0536(2)	0.3725(3)	0.1235(2)	0.119(10)	
O(17)	0.1686(2)	0.3518(2)	0.1053(2)	0.137(7)	
	0.1678(2)	0.3514(3)	0.1054(2)	0.133(10)	
O(18)	0.1410(2)	0.1941(2)	0.0838(2)	0.138(7)	
	0.1406(2)	0.1956(3)	0.0820(2)	0.135(10)	
O(19)	0.0461(2)	0.0926(2)	0.0894(2)	0.138(7)	
	0.0469(2)	0.0914(3)	0.0899(2)	0.130(10)	
O(20)	0.1545(2)	0.0336(2)	0.0907(2)	0.150(7)	
	0.1557(2)	0.0336(3)	0.0909(2)	0.146(10)	
O(21)	0.2556(2)	0.2515(2)	0.0784(2)	0.154(7)	
	0.2553(2)	0.2530(3)	0.0762(2)	0.140(10)	
O(22)	0.3908(2)	0.4970(2)	0.1262(2)	0.128(7)	
	0.3923(2)	0.4979(3)	0.1276(2)	0.143(9)	
O(23)	0.4640(2)	0.3712(2)	0.1235(2)	0.129(7)	
	0.4644(2)	0.3715(3)	0.1242(2)	0.120(10)	
O(24)	0.3477(2)	0.3531(2)	0.1064(2)	0.128(7)	
	0.3472(2)	0.3541(3)	0.1064(2)	0.130(10)	
O(25)	0.3721(2)	0.1942(2)	0.0844(2)	0.131(7)	
	0.3720(2)	0.1943(3)	0.0827(2)	0.134(10)	
O(26)	0.3598(2)	0.0348(2)	0.0908(2)	0.143(7)	
	0.3594(2)	0.0352(3)	0.0905(2)	0.139(10)	
O(27)	0.4668(2)	0.0937(2)	0.0918(2)	0.132(7)	
	0.4673(2)	0.0933(3)	0.0911(2)	0.129(10)	
O(28)	0.4801(2)	0.2717(2)	0.3817(2)	0.130(7)	
	0.4791(2)	0.2721(3)	0.3808(2)	0.125(10)	
O(29)	0.2993(2)	0.1252(2)	0.3697(2)	0.115(7)	
	0.2992(2)	0.1252(3)	0.3695(2)	0.115(10)	
O(30)	0.4179(2)	0.1404(2)	0.3712(2)	0.136(7)	
	0.4181(2)	0.1402(3)	0.3714(2)	0.127(10)	
O(31)	0.4164(2)	0.4063(2)	0.3921(2)	0.120(7)	
	0.4164(2)	0.4063(3)	0.3917(2)	0.114(10)	
O(32)	0.3011(2)	0.3946(2)	0.3830(2)	0.143(7)	
	0.3010(2)	0.3947(3)	0.3828(2)	0.131(10)	
O(33)	0.2399(2)	0.2616(2)	0.3740(2)	0.127(7)	
	0.2389(2)	0.2621(3)	0.3739(2)	0.123(10)	
O(34)	0.1811(2)	0.1229(2)	0.3691(2)	0.138(7)	
	0.1811(2)	0.1234(3)	0.3684(2)	0.116(10)	
O(35)	0.0634(2)	0.1422(2)	0.3725(2)	0.131(7)	
	0.0632(2)	0.1434(3)	0.3713(2)	0.124(10)	
O(36)	0.0018(2)	0.2722(2)	0.3841(2)	0.128(7)	
	0.0006(2)	0.2728(3)	0.3831(2)	0.127(10)	

Table 3. Continued.

Atom	x	y	z	ũ, Å	Pop.
O(37)	0.0676(2)	0.4058(2)	0.3937(2)	0.132(7)	
	0.0674(2)	0.4063(3)	0.3925(2)	0.129(10)	
O(38)	0.1826(2)	0.3964(2)	0.3853(2)	0.131(7)	
	0.1818(2)	0.3971(3)	0.3845(2)	0.130(10)	
O(39)	0.0201(2)	0.4958(2)	0.2247(2)	0.123(7)	
	0.0203(2)	0.4961(3)	0.2229(2)	0.121(10)	
O(40)	0.3931(2)	0.1955(2)	0.1991(2)	0.122(7)	
	0.3926(2)	0.1967(3)	0.1983(2)	0.127(10)	
O(41)	0.2701(2)	0.4893(2)	0.2172(2)	0.124(7)	
	0.2704(2)	0.4897(3)	0.2159(2)	0.116(10)	
O(42)	0.2654(2)	0.2891(2)	0.2006(2)	0.131(7)	
	0.2656(2)	0.2898(3)	0.2005(2)	0.124(10)	
O(43)	0.2681(2)	0.0850(2)	0.1933(2)	0.129(7)	
	0.2684(2)	0.0841(3)	0.1937(2)	0.119(10)	
O(44)	0.1401(2)	0.1912(2)	0.1978(2)	0.124(7)	
	0.1393(2)	0.1924(3)	0.1975(2)	0.118(10)	
O(45)	0.3550(2)	0.2826(2)	0.2868(2)	0.124(7)	
	0.3552(2)	0.2839(3)	0.2874(2)	0.119(10)	
O(46)	0.1093(2)	0.2850(2)	0.2880(2)	0.123(7)	1.0
	0.1092(2)	0.2856(3)	0.2895(2)	0.118(10)	1.0
Interlayer atoms:					
Ca	0.2292(2)	0.5584(2)	0.0003(3)	0.284(5)	0.5
	0.2309(2)	0.5613(3)	0.0010(4)	0.276(7)	0.5
K(1)	0.25	0.9720(8)	0.0	0.30(2)	0.263(9)
	0.2653(18)	0.9560(9)	−0.0030(22)	0.32(4)	0.188(5)
K(2)	0.0176(4)	0.9745(6)	0.0012(4)	0.21(2)	0.152(5)
	0.0182(6)	0.9721(8)	0.0012(5)	0.24(2)	0.192(4)
O(50)	0.2558(2)	0.4709(3)	0.0742(3)	0.242(7)	1.0
	0.2550(3)	0.4707(4)	0.0753(3)	0.24(1)	1.0
O(51)	0.1485(4)	0.4734(5)	0.0001(4)	0.22(1)	0.5
	0.1496(6)	0.4745(7)	0.0003(5)	0.21(2)	0.5
O(52)	0.1412(7)	0.6409(7)	0.0008(6)	0.33(2)	0.5
	0.1360(9)	0.6495(11)	−0.0009(7)	0.37(3)	0.5
O(53)	0.2467(102)	0.6981(8)	−0.0041(76)	0.38(2)	0.5
	0.2594(29)	0.6961(10)	−0.0036(18)	0.51(4)	0.5
O(54)	0.3361(6)	0.5479(11)	−0.0013(7)	0.35(2)	0.5
	0.3393(9)	0.5582(18)	0.0012(7)	0.47(3)	0.5
O(55)	0.1762(10)	0.8110(8)	0.0020(7)	0.39(2)	0.5
	0.1716(12)	0.8285(12)	−0.0003(7)	0.44(3)	0.5
O(56)	0.4100(12)	0.4461(11)	0.0015(7)	0.44(3)	0.5
	0.4098(18)	0.4543(15)	0.0021(9)	0.60(4)	0.5
O(57)	0.25	0.0928(18)	0.0	0.33(4)	0.33(2)
	0.25	0.1054(16)	0.0	0.30(4)	0.43(2)
O(58)	0.4781(17)	0.2807(26)	−0.0005(13)	0.64(5)	0.57(3)
	0.5000(27)	0.2932(26)	−0.0007(9)	0.67(5)	0.46(2)
O(59)	0.0402(8)	0.5529(12)	−0.0035(10)	0.61(3)	0.93(3)
	0.4670(12)	0.5607(20)	0.0092(12)	0.68(2)	0.67(4)
O(60)	0.3925(17)	0.7495(23)	−0.0023(12)	0.59(4)	0.5
	0.3837(16)	0.7969(16)	−0.0003(9)	0.59(4)	0.5

(1979). The octahedral sheet is trioctahedral and infinite in extent. As in other modulated layer silicates, such as antigorite (Zussman, 1954) and minnesotaite (Guggenheim and Eggleton, 1986), the octahedral sheet of bannisterite has a sinusoidal morphology (Figure 1). The modulation vector is parallel to *b*, and the wavelike nature of the sheet can be explained as a means of achieving congruency between the tetrahedral and octahedral sheets. The predominence of Fe^{2+} and Mn^{2+} within the octahedral sites enlarges the octahedral sheet beyond the dimensions found in ordinary micas. As

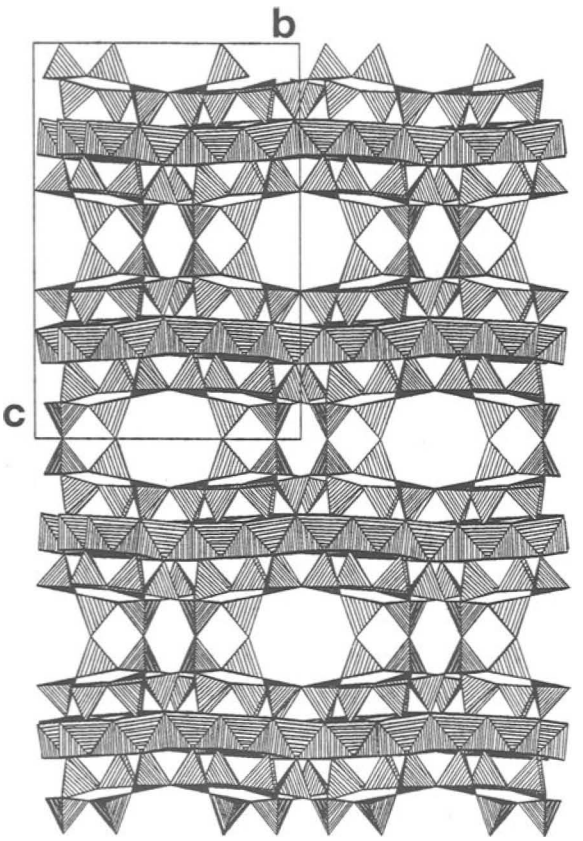

Figure 1. Projection on to the *b*–*c* plane of the framework of bannisterite showing wavelike character of the octahedral sheet, and the cross-linking via inverted tetrahedra.

noted by Guggenheim and Eggleton (1987, 1988), warping decreases the area on the concave side of the sheet to such an extent that a "normal" tetrahedral sheet can bond to the octahedral sheet in a mica-like fashion.

On the other side, the anions on the convex surface of a corrugated octahedral sheet are so spread apart that minor distortions of the tetrahedral sheet cannot overcome the dimensional mismatch. In bannisterite the tetrahedra maintain the continuity over these convex areas by reticulating into irregularly shaped 5-, 6-, or 7-fold rings (Figure 2). In addition, of the 16 unique tetrahedra, 4 in the 5- and 7-fold rings are directed toward the interlayer region, and the apical oxygen atoms of these tetrahedra [O(13), O(14)] are shared with similarly inverted tetrahedra from the adjacent layer (Figures 1–3). This cross-bonding of the layers of the bannisterite structure via inverted tetrahedra contributes to the brittle quality of the mineral.

Two minerals whose structures are closely related to that of bannisterite are ganophyllite and stilpnomelane. All three of these modulated layer silicates have modified 2:1 trioctahedral mica-like structures with some

https://doi.org/10.1346/CCMN.1992.0400201 Published online by Cambridge University Press

Table 4. Anisotropic thermal parameters for bannisterite. BH = Broken Hill; FF = Franklin Furnace. U values (Å^2) are multiplied by 100.

Atom		U_{11}	U_{22}	U_{33}	U_{12}	U_{13}	U_{23}
M(1)	BH	0.98(4)	1.37(3)	1.91(4)	−0.27(3)	0.26(3)	−0.23(3)
	FF	0.82(6)	0.83(5)	1.26(5)	−0.09(4)	0.00(4)	−0.10(4)
M(2)		0.77(4)	0.93(3)	1.86(4)	−0.06(3)	0.21(3)	0.04(3)
		0.63(5)	0.84(5)	1.17(5)	−0.08(4)	0.01(4)	−0.02(4)
M(3)		1.08(4)	1.04(3)	2.21(4)	0.02(3)	0.21(3)	0.08(3)
		0.70(6)	0.93(5)	1.43(5)	0.05(4)	0.00(4)	0.18(4)
M(4)		0.90(4)	1.04(3)	2.16(4)	−0.05(3)	−0.03(3)	−0.01(3)
		0.67(6)	0.76(5)	1.26(6)	−0.05(4)	−0.08(4)	−0.09(4)
M(5)		1.31(4)	1.19(3)	2.37(4)	0.03(3)	0.25(3)	−0.15(3)
		0.98(6)	0.91(5)	1.60(6)	−0.03(5)	−0.11(4)	−0.13(4)
M(6)		1.05(4)	1.10(3)	2.62(4)	0.03(3)	0.33(3)	0.07(3)
		0.79(5)	0.96(5)	1.80(5)	0.10(4)	0.02(4)	0.23(4)
M(7)		0.97(4)	1.03(3)	2.41(4)	0.13(3)	0.33(3)	0.17(3)
		0.75(5)	0.88(5)	1.63(6)	0.04(4)	0.66(4)	0.09(4)
M(8)		1.56(4)	1.65(4)	2.68(5)	0.14(3)	0.19(3)	0.41(3)
		0.85(6)	1.07(5)	1.61(6)	0.24(4)	0.03(5)	0.35(4)
M(9)		0.84(4)	0.89(3)	1.99(4)	0.14(3)	0.10(3)	0.14(3)
		0.74(5)	1.04(5)	1.48(5)	0.13(4)	0.00(4)	0.41(4)
M(10)		1.25(4)	1.12(3)	2.26(4)	0.17(3)	0.39(3)	0.17(3)
		0.92(5)	1.06(5)	1.53(5)	0.14(4)	0.00(4)	0.21(4)
Si(1)		0.96(7)	0.83(6)	0.96(6)	−0.16(5)	0.30(6)	−0.16(5)
		1.10(9)	0.90(8)	1.04(9)	−0.18(7)	0.04(7)	−0.12(7)
Si(2)		0.94(7)	0.85(6)	1.54(7)	0.18(5)	−0.08(6)	−0.10(5)
		1.08(9)	0.92(9)	1.07(9)	0.12(7)	−0.21(7)	−0.01(7)
Si(3)		0.74(7)	0.74(6)	1.36(7)	−0.03(5)	0.08(5)	−0.02(5)
		1.06(10)	0.84(8)	1.02(9)	−0.01(7)	−0.11(7)	−0.09(7)
Si(4)		0.86(7)	0.74(6)	1.55(7)	0.09(5)	0.01(6)	0.02(5)
		1.01(10)	0.95(8)	1.28(9)	0.05(7)	−0.19(7)	0.00(7)
Si(5)		0.72(7)	0.93(6)	1.68(7)	−0.11(5)	0.16(6)	−0.15(5)
		0.95(9)	0.96(8)	1.25(9)	−0.08(7)	−0.16(7)	−0.11(7)
Si(6)		0.55(6)	0.72(6)	1.39(7)	−0.03(5)	0.03(5)	0.05(5)
		0.90(9)	0.89(8)	1.20(9)	0.01(7)	−0.11(7)	0.12(7)
Si(7)		0.72(7)	0.68(6)	1.43(7)	−0.07(5)	0.08(6)	−0.02(5)
		0.95(9)	0.85(8)	1.18(9)	0.07(7)	−0.01(7)	0.02(7)
Si(8)		0.78(9)	0.69(6)	1.61(7)	−0.09(5)	0.21(6)	−0.13(5)
		0.78(9)	0.77(8)	1.33(9)	−0.02(7)	−0.14(7)	0.05(7)
Si(9)		0.66(6)	1.02(6)	1.63(7)	−0.05(5)	0.29(6)	−0.27(5)
		0.85(9)	1.04(8)	1.24(9)	0.13(7)	−0.05(7)	−0.16(7)
Si(10)		0.83(7)	0.68(6)	1.35(7)	−0.06(5)	0.12(6)	0.10(5)
		0.83(9)	0.82(8)	1.08(9)	−0.09(7)	−0.06(7)	0.04(7)
Si(11)		0.75(7)	0.73(6)	1.51(7)	−0.01(5)	0.20(6)	−0.12(5)
		0.86(9)	0.81(8)	1.08(9)	−0.08(7)	−0.03(7)	−0.11(7)
Si(12)		0.90(7)	0.99(6)	1.60(7)	−0.25(5)	0.39(6)	−0.27(5)
		1.11(10)	0.91(8)	1.21(9)	−0.06(7)	0.01(7)	−0.04(7)
Si(13)		1.19(7)	0.94(6)	1.34(7)	−0.02(5)	0.24(6)	0.05(5)
		1.41(10)	1.06(9)	1.13(9)	0.00(8)	0.15(7)	0.00(7)
Si(14)		1.26(7)	1.17(6)	1.45(7)	−0.04(6)	0.23(6)	−0.11(5)
		1.37(10)	1.26(9)	1.08(9)	0.04(8)	−0.06(7)	−0.09(7)
Si(15)		1.26(7)	1.16(6)	1.47(7)	0.02(5)	0.07(6)	−0.13(5)
		1.20(10)	1.40(9)	1.36(9)	0.03(8)	−0.12(7)	−0.14(8)
Si(16)		1.11(7)	0.88(6)	1.36(7)	−0.06(5)	0.11(6)	−0.01(5)
		1.06(10)	1.02(9)	1.09(9)	0.05(7)	−0.11(7)	0.01(7)
O(1)		1.54(19)	1.03(16)	1.89(19)	0.22(14)	0.50(16)	0.13(14)
		1.14(25)	1.12(22)	1.63(24)	−0.19(20)	−0.23(19)	0.17(19)
O(2)		1.36(18)	1.42(16)	1.37(18)	0.33(15)	0.13(15)	0.00(14)
		1.12(25)	1.17(23)	1.41(23)	−0.18(20)	0.15(19)	−0.14(18)
O(3)		1.19(18)	1.44(16)	1.43(19)	0.14(13)	0.24(15)	0.03(13)
		1.09(25)	1.00(22)	1.84(24)	0.19(19)	0.20(20)	−0.01(19)
O(4)		1.51(19)	2.01(17)	1.57(18)	0.44(15)	0.39(16)	0.30(14)
		1.16(25)	1.69(24)	1.63(24)	−0.02(20)	−0.06(20)	0.63(20)
O(5)		1.47(19)	1.73(17)	2.15(20)	0.52(15)	0.15(17)	0.06(14)
		1.12(26)	1.59(24)	2.08(26)	−0.14(21)	0.01(21)	0.06(20)
O(6)		0.84(17)	0.91(15)	1.63(18)	−0.03(13)	−0.06(15)	−0.08(13)
		1.19(25)	1.11(22)	1.13(22)	−0.10(20)	−0.09(18)	−0.21(18)

https://doi.org/10.1346/CCMN.1992.0400201 Published online by Cambridge University Press

Table 4. Continued.

Atom	U_{11}	U_{22}	U_{33}	U_{12}	U_{13}	U_{23}
O(7)	1.31(19)	1.49(16)	1.16(18)	−0.04(14)	0.09(15)	0.05(13)
	1.42(26)	0.94(22)	1.02(22)	0.00(19)	0.22(19)	−0.04(18)
O(8)	1.30(18)	1.05(16)	1.16(17)	0.09(13)	0.10(15)	−0.07(13)
	1.21(25)	1.09(22)	1.22(23)	−0.30(19)	−0.17(19)	−0.10(18)
O(9)	1.23(18)	1.53(17)	1.76(19)	0.07(14)	0.10(16)	−0.37(14)
	1.38(26)	1.15(23)	1.77(25)	−0.22(20)	0.16(20)	−0.10(19)
O(10)	1.27(18)	0.93(16)	1.56(19)	−0.17(13)	0.16(16)	−0.16(13)
	1.05(24)	1.08(22)	1.38(23)	−0.20(20)	−0.09(19)	0.05(19)
O(11)	1.00(18)	1.35(16)	1.43(18)	0.24(14)	0.39(15)	0.06(13)
	1.19(26)	1.26(23)	1.28(23)	−0.31(20)	0.22(19)	0.20(19)
O(12)	1.45(19)	2.17(17)	1.44(18)	−0.30(15)	0.15(16)	−0.13(15)
	1.34(26)	1.40(24)	1.61(24)	−0.65(20)	−0.04(20)	0.20(19)
O(13)	2.75(21)	2.93(20)	0.95(18)	−0.51(17)	−0.58(16)	−0.16(15)
	3.28(32)	2.38(28)	1.46(25)	−0.61(26)	−0.16(22)	0.05(22)
O(14)	2.29(21)	1.33(17)	1.92(19)	0.56(15)	−0.16(17)	0.17(14)
	1.96(30)	1.94(26)	2.15(26)	0.39(22)	−0.17(22)	0.10(22)
O(15)	2.00(20)	0.98(16)	1.34(18)	−0.18(14)	−0.15(16)	0.07(13)
	2.35(30)	1.11(23)	1.35(24)	−0.52(21)	−0.19(21)	0.15(19)
O(16)	1.24(18)	1.95(18)	1.67(19)	−0.79(15)	0.36(15)	0.18(14)
	1.47(26)	1.51(24)	1.30(23)	−0.51(21)	−0.36(19)	0.42(19)
O(17)	1.68(19)	1.55(17)	2.38(21)	−0.36(15)	0.50(17)	−0.41(15)
	1.93(29)	1.93(25)	1.45(24)	0.11(22)	−0.08(21)	0.09(20)
O(18)	1.73(20)	1.98(17)	2.03(20)	−0.06(15)	0.44(17)	0.09(15)
	1.71(28)	2.36(27)	1.32(24)	−0.08(23)	−0.10(21)	−0.24(21)
O(19)	1.48(19)	1.56(17)	2.69(21)	0.00(15)	0.80(17)	−0.23(15)
	2.07(28)	1.01(23)	2.03(26)	−0.32(22)	0.22(21)	−0.26(20)
O(20)	1.50(19)	1.62(17)	3.63(24)	−0.12(15)	0.70(19)	0.86(16)
	2.00(30)	1.68(25)	2.74(28)	−0.27(23)	0.59(23)	0.45(22)
O(21)	2.18(21)	2.05(18)	2.84(23)	0.34(16)	0.50(19)	0.07(16)
	1.66(28)	2.37(27)	1.89(26)	−0.16(22)	0.08(22)	−0.50(21)
O(22)	2.09(20)	1.10(16)	1.70(19)	0.07(15)	0.07(17)	−0.01(14)
	1.77(29)	1.30(23)	1.42(23)	0.27(20)	−0.27(20)	−0.02(19)
O(23)	1.40(19)	2.21(18)	1.35(18)	0.63(15)	0.23(16)	0.24(14)
	1.51(27)	1.66(24)	1.14(23)	0.72(21)	−0.03(19)	0.23(20)
O(24)	2.01(20)	1.71(18)	2.18(20)	0.10(15)	−0.14(17)	−0.46(15)
	1.50(27)	1.58(24)	1.99(25)	−0.35(21)	−0.53(21)	0.00(20)
O(25)	1.50(19)	1.75(17)	1.89(20)	−0.13(15)	0.20(16)	−0.07(14)
	1.73(28)	1.89(25)	1.74(25)	0.18(22)	−0.58(21)	−0.10(20)
O(26)	1.48(19)	1.60(17)	3.06(22)	0.45(15)	−0.16(18)	0.94(15)
	1.01(26)	2.05(26)	2.71(28)	0.04(22)	−0.59(22)	0.28(22)
O(27)	1.27(18)	1.13(17)	2.81(21)	0.10(14)	−0.50(17)	−0.50(14)
	0.82(24)	1.20(23)	2.95(28)	−0.05(20)	−0.76(20)	−0.29(21)
O(28)	2.51(21)	0.94(16)	1.66(19)	−0.18(15)	0.19(17)	−0.06(13)
	2.04(28)	1.25(23)	1.39(24)	−0.01(22)	−0.33(20)	0.01(19)
O(29)	0.77(17)	1.19(16)	2.03(20)	0.22(13)	0.25(15)	0.22(13)
	1.01(25)	1.45(24)	1.52(24)	0.31(20)	−0.22(19)	−0.06(19)
O(30)	1.36(19)	1.75(18)	2.45(21)	−0.78(15)	0.38(17)	0.04(15)
	1.57(27)	1.81(25)	1.44(24)	−0.44(21)	−0.44(20)	0.21(20)
O(31)	1.12(18)	1.89(17)	1.34(18)	0.32(14)	0.33(15)	−0.09(14)
	1.18(25)	1.73(24)	1.01(22)	0.30(21)	0.06(18)	0.10(19)
O(32)	1.36(20)	1.95(17)	2.83(22)	−0.24(15)	0.22(17)	0.34(15)
	1.36(26)	2.14(26)	1.66(24)	−0.39(22)	−0.45(20)	0.73(21)
O(33)	2.30(20)	1.07(16)	1.48(19)	−0.06(15)	−0.08(17)	−0.00(13)
	2.13(28)	1.05(22)	1.32(23)	−0.16(21)	−0.37(20)	−0.23(19)
O(34)	1.35(18)	1.43(17)	1.79(19)	−0.43(14)	0.31(16)	0.11(13)
	1.51(27)	1.35(23)	1.15(23)	−0.19(20)	−0.36(19)	0.27(19)
O(35)	1.23(18)	1.64(17)	2.29(21)	0.44(15)	0.30(16)	−0.31(15)
	1.36(27)	1.72(25)	1.51(24)	0.47(21)	−0.28(20)	−0.38(20)
O(36)	1.81(19)	1.16(16)	1.97(19)	0.06(15)	−0.10(17)	−0.19(14)
	2.45(29)	1.03(22)	1.38(24)	−0.02(22)	−0.25(21)	0.04(19)
O(37)	1.12(19)	1.42(17)	2.67(21)	−0.55(14)	0.64(17)	−0.24(15)
	1.73(27)	1.53(24)	1.75(25)	−0.16(22)	−0.17(20)	0.50(20)
O(38)	1.17(18)	2.20(18)	1.76(19)	0.44(15)	0.22(16)	−0.04(15)
	1.67(27)	1.93(25)	1.50(24)	0.60(22)	0.07(20)	0.04(20)

https://doi.org/10.1346/CCMN.1992.0400201 Published online by Cambridge University Press

Table 4. Continued.

Atom	U_{11}	U_{22}	U_{33}	U_{12}	U_{13}	U_{23}
O(39)	1.04(18)	1.35(16)	2.18(19)	−0.27(14)	0.26(16)	−0.27(14)
	1.93(29)	1.07(23)	1.36(23)	−0.14(20)	0.01(20)	−0.01(19)
O(40)	1.14(18)	1.50(16)	1.83(19)	0.14(14)	0.54(16)	−0.23(14)
	1.84(28)	1.14(23)	1.86(25)	0.41(21)	0.20(21)	−0.06(20)
O(41)	1.00(18)	1.02(16)	2.62(21)	−0.08(13)	0.45(16)	0.36(14)
	1.58(28)	0.97(22)	1.51(24)	0.24(20)	0.18(20)	−0.04(19)
O(42)	1.83(20)	1.06(16)	2.28(20)	−0.31(14)	0.40(17)	0.19(14)
	1.39(27)	1.61(24)	1.60(24)	0.28(21)	−0.05(20)	0.60(20)
O(43)	1.72(19)	1.36(17)	1.92(20)	0.13(14)	0.27(17)	−0.16(14)
	1.62(27)	1.52(23)	1.13(23)	0.13(21)	−0.05(19)	0.09(19)
O(44)	1.52(19)	1.49(16)	1.62(19)	−0.28(15)	0.18(16)	−0.03(14)
	1.51(26)	1.35(23)	1.29(23)	−0.33(21)	−0.15(20)	−0.03(19)
O(45)	0.78(18)	1.57(17)	2.23(20)	0.01(14)	0.01(16)	0.03(14)
	1.48(26)	1.31(23)	1.43(24)	0.04(20)	−0.14(20)	−0.07(19)
O(46)	1.35(19)	1.11(16)	2.08(20)	−0.21(14)	0.13(16)	0.15(14)
	1.56(26)	1.24(23)	1.39(24)	−0.19(21)	−0.12(20)	−0.19(19)
Ca	7.7(3)	4.4(2)	12.1(3)	−0.8(2)	0.4(4)	−0.8(2)
	7.5(6)	4.4(2)	11.0(4)	−1.1(2)	0.0(6)	0.0(3)
K(1)	10.7(1.1)	13.3(1.2)	3.6(6)	0.0	−0.7(7)	0.0
	11.9(3.6)	10.6(1.2)	8.0(1.4)	0.8(1.4)	−5.5(2.1)	−1.1(1.5)
K(2)	4.2(8)	7.0(9)	2.7(5)	−5.1(5)	0.4(6)	−0.7(6)
	5.6(1.1)	9.7(1.4)	2.2(5)	−6.2(8)	−0.8(7)	0.5(8)
O(50)	3.3(3)	2.6(2)	11.7(5)	−0.1(2)	1.1(4)	−1.5(3)
	4.1(5)	4.0(4)	8.7(6)	−0.5(3)	−0.4(4)	−1.8(4)
O(51)	4.4(6)	5.3(6)	4.3(6)	−0.1(5)	−0.4(5)	0.8(5)
	4.9(9)	3.9(7)	4.0(7)	1.0(7)	−0.3(6)	0.1(6)
O(52)	16.6(1.5)	7.1(7)	8.4(1.0)	4.0(9)	1.6(1.2)	−1.3(8)
	13.4(2.0)	14.2(1.7)	12.9(1.7)	4.7(1.7)	−1.2(1.4)	0.6(1.5)
O(53)	27.5(4.2)	6.6(6)	8.4(6.8)	−2.5(4.4)	2.5(4.7)	−2.0(2.3)
	58.1(5.7)	11.8(1.4)	7.2(1.3)	−21.6(3.1)	6.4(2.2)	−4.4(1.7)
O(54)	6.6(9)	20.8(1.6)	9.1(1.2)	4.1(1.1)	0.6(1.0)	0.3(1.2)
	9.4(1.8)	50.3(4.4)	7.7(1.5)	0.4(2.6)	−0.8(1.3)	−2.3(2.2)
O(55)	31.8(2.5)	7.5(9)	7.2(1.1)	−2.5(1.3)	−2.6(1.6)	0.3(8)
	34.5(3.6)	19.5(2,2)	2.8(1.0)	−8.9(2.3)	−1.8(1.6)	−0.1(1.2)
O(56)	38.6(3.2)	14.3(1.4)	6.3(1.1)	−15.0(2.0)	−1.6(1.7)	0.2(1.0)
	74.0(7.8)	24.5(3.8)	9.1(1.9)	2.9(4.3)	12.3(3.9)	2.8(2.2)
O(57)	7.4(2.3)	14.8(3.1)	9.7(2.7)	0.0	1.8(2.1)	0.0
	6.7(2.1)	11.0(2.5)	10.0(2.4)	0.0	−3.1(1.7)	0.0
O(58)	31.9(4.8)	76.3(8.4)	14.3(2.5)	7.9(4.0)	5.8(3.2)	−11.6(3.3)
	74.0(10.0)	61.1(7.5)	0.7(1.1)	33.8(6.8)	−1.0(2.7)	−0.5(2.4)
O(59)	30.4(2.5)	45.8(3.4)	36.2(3.7)	19.2(2.0)	3.9(2.6)	9.6(2.6)
	26.2(4.0)	69.5(8.0)	38.3(4.1)	−33.0(4.0)	15.1(3.1)	−21.4(4.3)
O(60)	31.5(4.1)	62.7(7.6)	9.9(2.0)	−11.9(3.9)	1.7(2.9)	−5.0(3.0)
	29.9(5.0)	55.6(5.7)	18.4(3.0)	−14.2(4.6)	−4.2(2.9)	0.3(3.3)

of the tetrahedra inverted away from the octahedral sheet and bonded to inverted tetrahedra from an opposite layer. In stilpnomelane these inverted tetrahedra form six-membered rings that separate islands containing seven six-membered rings of an ordinary mica sheet (Eggleton, 1972). By contrast, the inverted tetrahedra in ganophyllite occur as isolated pairs, and the tetrahedral sheet contains uninterrupted pyroxene-like tetrahedral chains bonded to the octahedral sheet (Eggleton and Guggenheim, 1986). Guggenheim and Eggleton (1987, 1988) referred to stilpnomelane as an "island-like" structure, and to ganophyllite as a "strip-like" structure (Figure 3).

The more general concept of the "homologous series" in modulated layer silicates as proposed by Guggenheim and Eggleton (1988), comprising mica-like species characterized by the presence of certain tetrahedra that are inverted and cross-linked to similar tetrahedra in opposite layers, loosely accommodates the bannisterite structure. As noted by Guggenheim and Eggleton (1987, 1988), bannisterite does not fit easily into either the "island-like" or "strip-like" structural categories. The four inverted tetrahedra of bannisterite do not themselves form a complete hexagonal ring, nor do they isolate islands of normally directed tetrahedra. At the same time, the tetrahedral sheets of bannisterite lack the straight one-dimensional strips that characterize ganophyllite and minnesotaite.

Also, the structures of bannisterite, stilpnomelane, and ganophyllite do not appear to share a simple polysomatic relationship, that is, they are not built up of various linkages of a few simple subunits, as described

for pyriboles by Thompson (1978). A comparison of the octahedral sheet of bannisterite with those of zussmanite, ganophyllite, and stilpnomelane (Figure 3) reveals a number of structural motifs that are shared among these modulated layer silicates. These modules may or may not have a genetic significance, but they do suggest that when these structures occur together, they may intergrow topotactically. The degree with which these minerals do intergrow and the nature of any intermediate defect structures remains to be determined by high-resolution transmission electron microscopy.

In the following discussion reference may be made to Tables 7 and 8 for bond lengths and other interatomic distances.

Octahedral and tetrahedral cation distributions

Dunn *et al.* (1981) speculate on the basis of microprobe analyses of several bannisterite specimens from Franklin Furnace that Zn, Mg, and Fe^{2+} are ordered among the octahedral sites. Four types of octahedral sites can be distinguished on the basis of hydroxyl environment: the M(8) site is bonded to one hydroxyl group; the M(1), M(2), M(3), M(9), and M(10) sites are surrounded by two hydroxyl groups; and the M(7) site by four hydroxyl groups. However, plots of the number of coordinating hydroxyl groups versus the average bond lengths (Table 8) reveal no systematic relationship. Moreover, there appears to be no obvious pattern to the spatial distribution of the octahedra in terms of size or estimated occupancy. In the Franklin Furnace crystals for example, if one site were fully occupied by Mg, the apparent occupancy parameter for that site would be 0.49; similarly, if one site were fully occupied by Zn, its apparent occupancy would be 1.29. Therefore, our structure refinements have provided no clear evidence for preferential partitioning of Mg or Zn among the octahedral sites in either the Broken Hill or Franklin Furnace bannisterites.

The bond lengths for the octahedra vary from 2.060 to 2.401 Å, and the average distances from 2.139 to 2.237 Å. In the tetrahedra, the distances vary from 1.594 to 1.706 Å; the averages vary from 1.607 to 1.690 Å, but for T(1) to T(12) only, the highest average is 1.623 Å. All these variations are considerable, but the corresponding individual distances for Broken Hill and Franklin Furnace are remarkably consistent, about equal to the error of determination (±0.003).

In the silicate layer the average Si–O bond lengths in the 12 tetrahedra linked to the octahedral sheet are all close to 1.614 Å (±0.004) in both structures (Table 8). The inverted tetrahedra are significantly larger, indicating a concentration of Al in these sites. The fraction, x, of Al in each site may be estimated by the linear relationship: $x_{Al} = 6.4116D - 10.282$, where D is the average T–O distance (Jones, 1968). The distribution so obtained is given in Table 9. The total

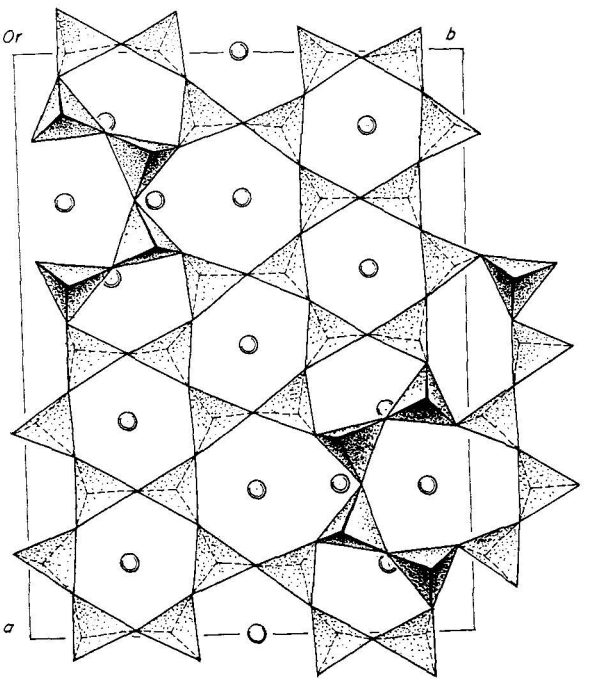

Figure 2. Projection of the tetrahedral sheet normal to the a–b plane, immediately below the level $z = 0$. Distorted 5-, 6-, and 7-fold rings can be seen in relation to the tetrahedra. Circles are OH groups in the octahedral sheet.

amounts of Al indicated by this method are somewhat less than the experimentally-determined compositions, which are 1.43 for Broken Hill, and 1.48 for Franklin Furnace. Nevertheless, it seems clear that Al in bannisterite is preferentially partitioned into the central pair of inverted tetrahedral quartets.

It is not certain whether Al is concentrated into cross-linking tetrahedra in all or only some modulated layer silicates. The only other structure determination of a modulated 2:1 layer silicate that gives any experimental evidence for the location of Al atoms is that of zussmanite (see Figure 3) by Lopes-Vieira and Zussman (1969). These authors refined the structure by least-squares methods using film-measured data, and they found that the average of T–O distances in the three cross-linking tetrahedra is 1.65 Å. The average T–O bond length in the tetrahedra adjacent to the octahedral sheet is 1.61 Å, and so it appears that Al occurs primarily in the inverted tetrahedra in zussmanite as well as in bannisterite. On the other hand, Eggleton and Guggenheim (1986) have argued that in ganophyllite Al should be partitioned into the normally directed tetrahedral strips to facilitate coordination with the expanded octahedral sheet. Proof of this assertion awaits a high-resolution refinement of the ganophyllite crystal structure.

The location of the minor amount of Fe^{3+} found in

https://doi.org/10.1346/CCMN.1992.0400201 Published online by Cambridge University Press

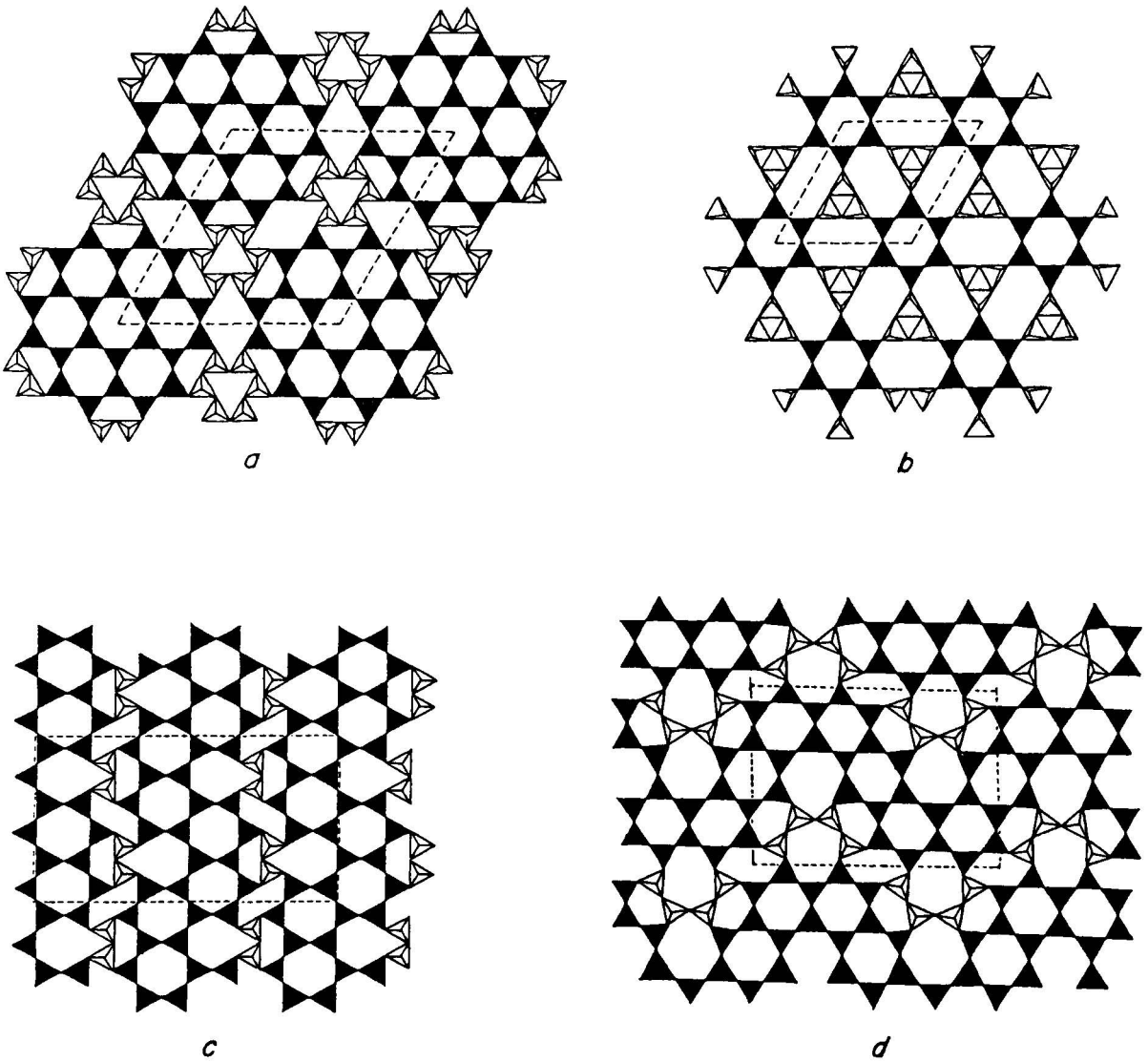

Figure 3. Schematic outlines of silicate sheets for various modulated layer structures: (*a*) stilpnomelane; (*b*) zussmanite; (*c*) ganophyllite; (*d*) bannisterite (after Guggenheim and Eggleton, 1986).

bannisterite by Smith and Frondel (1968) is not clear. Dunn *et al.* (1981) speculate that trivalent Fe may occupy the tetrahedral rather than the octahedral sites since formulas for both the Broken Hill and Franklin Furnace bannisterites indicate a small deficiency of (Si,Al) atoms and an excess of octahedral cations. Because the inclusion of ferric iron in the large inverted tetrahedra seems structurally reasonable, we concur that the ferric iron in bannisterite is probably tetrahedrally coordinated. The results of recent Mössbauer spectroscopy experiments on bannisterite support this interpretation (E. A. Ferrow, personal communication). Unfortunately, we do not have information about the valency of Fe in the bannisterite from Broken Hill.

Interlayer cations and water molecules

Although it appears that Al particularly favors 2 of the 16 tetrahedral sites, the analyses of Dunn *et al.* (1981) indicate that the aluminum content is consistently close to 1.5 atoms per asymmetric unit. Therefore, the two inverted tetrahedra into which Al is concentrated cannot be fully occupied with respect to Al. These tetrahedra, T(14) and T(15), form a ring of 4 in the *a*–*c* plane with their symmetrically-related counterparts, to which they are attached via the shared apical oxygen atom O(14). The stoichiometry suggests that, on average, three of these four tetrahedra contain Al while the fourth contains Si. Presumably, each tetra-

https://doi.org/10.1346/CCMN.1992.0400201 Published online by Cambridge University Press

Table 7. Bond lengths in the bannisterite framework. BH = Broken Hill; FF = Franklin Furnace.

Atoms	BH	FF	Atoms	BH	FF
Octahedral cations: ±0.004 Å (BH); ±0.005 Å (FF)					
M(1)–O(39)	2.089	2.120	M(2)–O(46)	2.084	2.115
–O(9)	2.121	2.136	–O(44)	2.104	2.094
–O(11)	2.126	2.127	–O(12)	2.135	2.148
–O(46)	2.136	2.123	–O(11)	2.144	2.136
–O(12)	2.184	2.183	–O(10)	2.226	2.231
–O(1)	2.195	2.173	–O(11)′	2.240	2.218
M(3)–O(41)	2.133	2.154	M(4)–O(44)	2.090	2.088
–O(6)	2.147	2.160	–O(42)	2.102	2.081
–O(9)	2.177	2.188	–O(46)	2.127	2.178
–O(43)	2.191	2.180	–O(8)	2.135	2.138
–O(8)	2.199	2.198	–O(1)	2.151	2.150
–O(1)	2.283	2.297	–O(7)	2.226	2.240
M(5)–O(43)	2.126	2.124	M(6)–O(41)	2.060	2.075
–O(44)	2.160	2.158	–O(45)	2.131	2.121
–O(5)	2.169	2.195	–O(42)	2.151	2.122
–O(7)	2.180	2.178	–O(2)	2.175	2.157
–O(41)	2.185	2.224	–O(8)	2.212	2.194
–O(10)	2.217	2.213	–O(5)	2.324	2.368
M(7)–O(40)	2.108	2.108	M(8)–O(39)	2.138	2.177
–O(42)	2.107	2.102	–O(10)	2.131	2.165
–O(43)	2.159	2.154	–O(4)	2.160	2.164
–O(7)	2.168	2.168	–O(5)	2.194	2.179
–O(45)	2.188	2.226	–O(2)	2.360	2.368
–O(6)	2.227	2.242	–O(12)	2.401	2.367
M(9)–O(2)	2.105	2.099	M(10)–O(40)	2.079	2.090
–O(3)	2.112	2.116	–O(39)	2.098	2.132
–O(45)	2.113	2.120	–O(4)	2.204	2.181
–O(3)′	2.164	2.149	–O(6)	2.210	2.214
–O(40)	2.177	2.162	–O(3)	2.280	2.304
–O(4)	2.331	2.385	–O(9)	2.380	2.350
Tetrahedral distances: ±0.004 Å (BH); ±0.005 Å (FF)					
Si(1)–O(17)	1.605	1.598	Si(2)–O(24)	1.594	1.604
–O(1)	1.611	1.609	–O(2)	1.607	1.621
–O(15)	1.624	1.615	–O(22)	1.619	1.618
–O(16)	1.637	1.632	–O(23)	1.621	1.620
Si(3)–O(30)	1.607	1.605	Si(4)–O(27)	1.601	1.602
–O(28)	1.608	1.605	–O(4)	1.613	1.616
–O(3)	1.611	1.608	–O(31)	1.618	1.605
–O(23)	1.624	1.625	–O(28)	1.616	1.618
Si(5)–O(32)	1.609	1.603	Si(6)–O(15)	1.612	1.623
–O(20)	1.617	1.611	–O(6)	1.608	1.608
–O(31)	1.617	1.630	–O(30)	1.616	1.624
–O(5)	1.626	1.610	–O(29)	1.631	1.623
Si(7)–O(33)	1.607	1.618	Si(8)–O(32)	1.608	1.615
–O(7)	1.620	1.600	–O(38)	1.606	1.613
–O(29)	1.618	1.628	–O(8)	1.606	1.604
–O(34)	1.622	1.612	–O(33)	1.608	1.609
Si(9)–O(26)	1.609	1.617	Si(10)–O(10)	1.622	1.600
–O(38)	1.610	1.609	–O(22)	1.617	1.607
–O(9)	1.618	1.609	–O(34)	1.621	1.626
–O(37)	1.622	1.613	–O(35)	1.628	1.620
Si(11)–O(11)	1.608	1.610	Si(12)–O(19)	1.596	1.600
–O(36)	1.609	1.602	–O(36)	1.619	1.627
–O(16)	1.621	1.615	–O(12)	1.619	1.619
–O(35)	1.614	1.605	–O(37)	1.619	1.622
Si(13)–O(13)	1.612	1.617	Si(14)–O(14)	1.655	1.639
–O(18)	1.625	1.634	–O(21)	1.652	1.650
–O(20)	1.632	1.644	–O(18)	1.679	1.661
–O(19)	1.642	1.636	–O(17)	1.694	1.684
Si(15)–O(21)	1.671	1.674	Si(16)–O(13)	1.603	1.602
–O(14)	1.674	1.687	–O(25)	1.615	1.601
–O(25)	1.691	1.693	–O(26)	1.623	1.625
–O(24)	1.704	1.706	–O(27)	1.624	1.636

https://doi.org/10.1346/CCMN.1992.0400201 Published online by Cambridge University Press

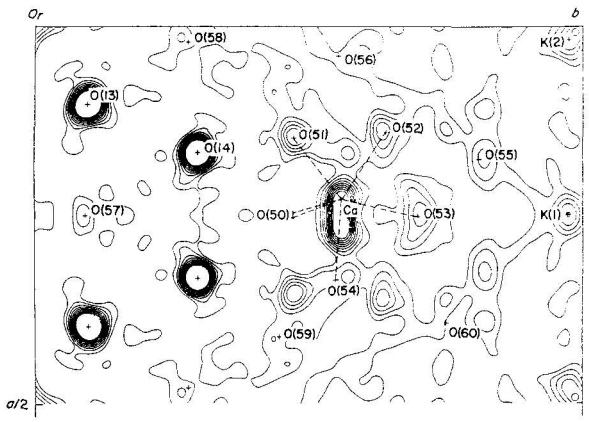

Figure 4. Electron density map of the section at $z = 0$ of bannisterite from Broken Hill, showing asymmetrical distribution of cations and water molecules in the interlayer region.

hedral site within the four-membered ring has an equal probability of containing the Si cation, so that over long ranges Si will be disordered over these sites. However, on a local scale, the presence of an odd Si cation will contribute to a charge imbalance in the surrounding interlayer area. This localized polarization appears to exert a strong effect on the interlayer sites.

As can be seen in an electron density map of the interlayer region at $z = 0$ (Figure 4), the electron density maximum for Ca is clearly split, and on refinement Ca is shifted about 0.3 Å away from the 2-fold axis. Although this condition may sometimes indicate that the structure has been refined in a space group with too high an order of symmetry, an attempt to refine in space group *Aa* did not yield an improved result. The absence of piezoelectric character in bannisterite (Smith and Frondel, 1968) also implies that the structure is genuinely centrosymmetric.

We interpret the splitting of the Ca position as a response to variations in the local Al/Si configuration. Since the bonds within the tetrahedra containing Al will be undersaturated, the interlayer cations might be expected to shift towards the aluminous tetrahedra and away from the tetrahedron containing Si. This shift will occur primarily in the $\pm a$ direction, since movement normal to the layers is constrained by the fully-occupied water molecules O(50) lying above and below the Ca position.

In addition to these latter two water molecules, each Ca cation is coordinated to four water molecules [O(51)–O(54)] lying in the $z = 0$ plane. The disorder over the Ca site influences, in turn, the positions and occupancies (in $A2/a$) of these coplanar waters, as shown schematically in Figure 5. Because of the 2-fold rotation axis at $x = 0.25$, the water molecules O(51)–O(54) occupy two sites within the zero-layer asymmetrical unit. However, depending on the Ca position, structural constraints indicate that within a single asymmetric cell only half of these sites can be filled. For instance, when $x_{Ca} = 0.23$, the bond length from Ca to one of the O(54) positions is unreasonably short (1.46 Å), and the bond lengths from Ca to one of the two O(51)-positions and one of the two O(52)-positions are too long (3.08 and 3.16 Å). On the other hand, the bond lengths from Ca at $x = 0.23$ to the corresponding oxygen atoms related by the 2-fold rotation axis are quite acceptable. Bond distances from Ca to the symmetrically-related O(54), O(51), and O(52) positions are 2.35, 2.33, and 2.39 Å, respectively. O(53) lies so close to the 2-fold axis that its distance to Ca is 2.31 Å in either case (Table 10).

Table 8. Average distances in framework octahedra and tetrahedra, in Ångstrom units. BH = Broken Hill, FF = Franklin Furnace.

Octahedra	BH	FF	Tetrahedra	BH	FF
M(1)	2.142	2.144	T(1)	1.619	1.614
M(2)	2.156	2.157	T(2)	1.610	1.616
M(3)	2.188	2.196	T(3)	1.613	1.611
M(4)	2.139	2.146	T(4)	1.612	1.610
M(5)	2.173	2.182	T(5)	1.617	1.614
M(6)	2.176	2.173	T(6)	1.617	1.620
M(7)	2.160	2.167	T(7)	1.617	1.615
M(8)	2.231	2.237	T(8)	1.607	1.610
M(9)	2.167	2.172	T(9)	1.615	1.612
M(10)	2.209	2.212	T(10)	1.622	1.613
Average	2.174	2.179	T(11)	1.613	1.608
			T(12)	1.613	1.617
			T(13)	1.628	1.633
			T(14)	1.670	1.659
			T(15)	1.685	1.690
			T(16)	1.616	1.616
			Average	1.623	1.622
			Average T(1)–T(12)	1.615	1.613

https://doi.org/10.1346/CCMN.1992.0400201 Published online by Cambridge University Press

Table 9. Aluminum occupancy in inverted tetrahedra. Fraction Al, $x_{Al} = 6.4116D - 10.282$ (Jones, 1968).

	Broken Hill		Franklin Furnace	
	D, A	x_{Al}	*D*	x_{Al}
T(13)	1.628	0.156	1.633	0.188
T(14)	1.670	0.425	1.659	0.355
T(15)	1.685	0.522	1.690	0.554
T(16)	1.616	0.079	1.616	0.079
Total Al		1.182		1.176

Therefore, it appears that the locations of the interlayer water molecules surrounding the Ca position are determined by the position of the Ca cation. Moreover, like the Ca site, these interlayer water sites are fully occupied on a local scale and half occupied when averaged over the entire structure. This interpretation finds strong support in the refined population parameters for these four water species: the average occupancy for the O(51), O(52), O(53), and O(54) sites is 0.56 in the Broken Hill bannisterite and 0.48 in the Franklin Furnace bannisterite. These parameters were held at 0.5 in the last least-squares cycles.

Threadgold (1979) observed positional disorder of the K cation at the origin, but he did not mention the extreme disorder exhibited by Ca and its coordinated water molecules as well. In light of the precise refinement he reported ($R = 0.029$), it is possible that he did not observe so high a degree of disorder in his partially dehydrated crystal. However, we emphasize that the similarity of interlayer disorder found in bannisterite crystals from both Franklin Furnace and Broken Hill is quite remarkable.

Comparison of refined occupancies with analytical values

In general, the occupancies for the interlayer cations determined by this X-ray refinement agree closely with the analytical values measured by Dunn *et al.* (1981). The occupancies found for Ca of 0.435 (Broken Hill) and 0.485 (Franklin Furnace) are quite close to the measured values of 0.40 and 0.50 (in the refinement these were both held to 0.5). Population parameters for K are not as concordant with the chemistry. The potassium cation, K(1), was assigned to a prominent peak on the 2-fold axis and refined to an occupancy of 0.263 for the Broken Hill crystal. In the Franklin Furnace crystal, K(1) appeared as a strongly-elongated peak and was refined in general position to an occupancy of 0.188. K(1) is loosely held among 8 framework oxygen atoms at an average distance of 3.36 Å, and one water molecule, O(55), at 3.10 Å. The other potassium cation, K(2), is displaced from a symmetry center at the origin and attains a local occupancy of 0.152 (Broken Hill) and 0.192 (Franklin Furnace). This cation is bound by 8 framework oxygen atoms at an average distance

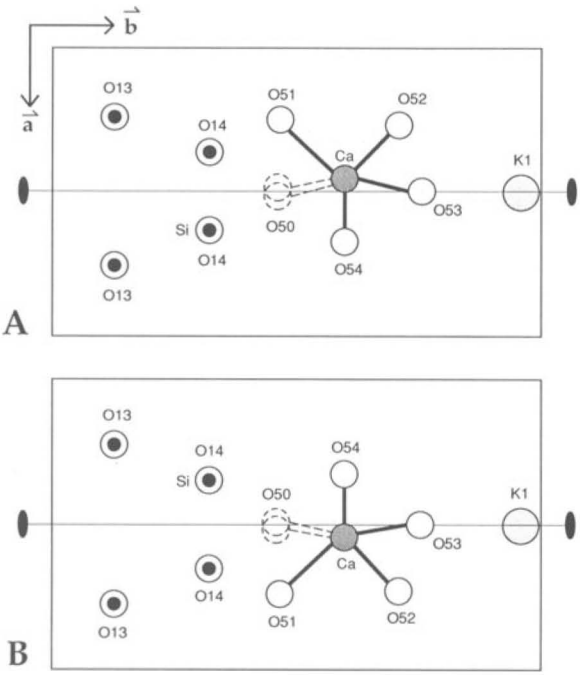

Figure 5. Schematic diagrams illustrating the positional disorder of the interlayer species. O(13) and O(14) represent apical oxygens shared by inverted tetrahedra above and below the plane $z = 0$. O(50) is a fully-occupied water species located 1.84 Å above and below this plane. When a Si cation is located in (A), the Ca cation is displaced along the opposite direction, and the O(51)–O(54) sites occupied are those indicated. Positioning of Si on the other side of the 2-fold axis produces the configuration shown in (B).

of 2.94 Å. Its thermal anisotropy is extreme (elongated toward the symmetry center), but its average thermal vibration is significantly less than that of K(1) (Table 3). In the Broken Hill material, these two K cations contribute 0.28 atoms to the refined formula unit, and for Franklin Furnace the sum is 0.38. These sums are both substantially less than the analytical values for (K,Na) of 0.41 and 0.49, respectively.

In addition to the Ca-coordinated water molecules, three more waters were assigned to distinct peaks in the difference maps during the structure analysis. These atoms [O(55), O(56), and O(57)] refined stably, and showed substantially higher thermal motion than the waters associated with calcium, but with slightly lower occupancies. O(57) lies on the 2-fold axis and presumably cannot be present when K(1) is present.

Lastly, three water molecules [O(58)–O(60)] were assigned to more diffuse maxima in the final difference maps. These positions refined stably but exhibited very large and eccentric thermal motions (Tables 4 and 5). These maxima probably represent electron density contributed by highly disordered water molecules, and their site definition is very uncertain. The thermal ellipsoids for all interlayer atoms (compared with those

https://doi.org/10.1346/CCMN.1992.0400201 Published online by Cambridge University Press

Table 10. Interatomic distances for the interlayer atoms in bannisterite.

Atoms	BH	FF	Atoms	BH	FF
Interlayer cations					
Ca[–Ca	1.47(2)	0.86(1) Å]	K(1)[–O(57)	1.98(3)	2.47(3)]
–O(50)	2.36(1)	2.39(1)	(2×)–O(20)	3.35(1)	3.28(5)
–O(50)′	2.37(1)	2.44(1)	(2×)–O(26)	3.46(1)	3.35(1)
–O(51)	2.27(1)	2.30(1)	(2×)–O(32)	3.42(1)	3.42(1)
–O(52)	2.39(2)	2.56(2)	(2×)–O(38)	3.33(1)	3.48(1)
–O(53)	2.33(4)	2.30(3)	(2×)–O(55)	3.11(2)	3.10(2)
–O(54)	2.39(2)	2.42(2)			
			K(2)[–K(2)	0	1.14(2)]
			–O(13)	2.78(1)	2.78(1)
			–O(13)′	2.94(1)	2.94(1)
			–O(19)	2.77(1)	2.77(1)
			–O(19)′	2.94(1)	2.94(1)
			–O(27)	2.81(1)	2.81(1)
			–O(27)′	3.04(1)	3.04(1)
			–O(31)	3.12(1)	3.11(1)
			–O(37)	3.15(1)	3.15(1)
Water molecules [O(50–60), max. 3.5 Å]					
O(50)–O(15)	3.18(1)	3.16(1)	O(51)–O(14)	2.90(1)	2.87(1)
–O(17)	2.90(1)	2.89(1)	–O(15)	3.17(1)	3.18(1)
–O(22)	3.21(1)	3.25(1)	–O(17)	3.27(1)	3.29(1)
–O(24)	2.88(1)	2.86(1)	–O(22)	3.19(1)	3.24(1)
–O(29)	3.17(1)	3.15(1)	–O(24)	3.28(1)	3.29(1)
–O(34)	3.13(1)	3.15(1)	–O(50)	2.89(1)	2.88(1)
–O(51)	2.89(1)	2.88(1)	–O(50)′	2.91(1)	2.93(1)
–O(51)′	2.91(1)	2.93(1)	–O(52)	2.75(1)	2.88(2)
–O(54)	2.91(1)	3.07(1)	–O(59)	2.74(1)	2.95(3)
–O(54)′	2.96(1)	3.07(1)			
O(52)–O(29)	3.36(2)	3.42(2)	O(53)–O(33)	3.4(2)	3.37(4)
–O(34)	3.43(1)	3.42(2)	–O(52)	2.5(2)	2.86(7)
–O(35)	3.48(1)	3.48(2)	–O(54)	3.1(2)	3.15(5)
–O(51)	2.75(1)	2.88(2)	–O(55)	2.5(2)	2.93(5)
–O(53)	2.7(2)	2.86(6)	–O(60)	3.4(2)	3.22(7)
–O(59)	2.67(2)	2.71(3)			
O(54)–O(15)	3.31(2)	3.41(2)	O(55)–O(32)	3.15(2)	3.11(2)
–O(22)	3.38(2)	3.40(2)	–O(38)	3.20(2)	3.08(2)
–O(29)	3.44(2)	3.48(2)	–O(52)	2.89(2)	3.04(3)
–O(34)	3.47(2)	3.45(2)	–O(53)	2.5(2)	2.93(5)
–O(53)	3.1(1)	3.15(5)			
–O(56)	2.34(2)	2.31(6)			
O(56)–O(14)	2.96(2)	3.03(3)	O(57)–O(13)	3.27(1)	3.28(1)
–O(15)	3.29(2)	3.29(3)	(2×)–O(20)	3.34(1)	3.40(1)
–O(16)	3.41(2)	3.42(3)	(2×)–O(21)	3.23(2)	3.06(2)
–O(17)	3.42(2)	3.50(3)	(2×)–O(26)	3.32(1)	3.38(1)
–O(22)	3.24(2)	3.23(2)			
–O(23)	3.37(2)	3.44(3)			
–O(24)	3.38(2)	3.43(3)			
–O(54)	2.34(3)	2.32(4)			
–O(58)	3.12(5)	3.32(6)			
–O(59)	2.91(3)	2.79(5)			
O(58)–O(14)	3.27(4)	3.42(3)	O(59)–O(51)	2.74(2)	2.95(3)
–O(16)	3.38(3)	3.48(3)	–O(52)	2.66(2)	2.71(3)
–O(23)	3.44(5)	3.15(3)	–O(56)	2.91(3)	2.79(5)
–O(28)	3.11(3)	3.32(6)	–O(58)	3.07(5)	2.64(4)
–O(56)	3.12(5)	2.51(5)	–O(59)	3.05(5)	2.51(5)
–O(59)	3.05(5)				
O(60)–O(53)	3.3(2)	3.22(7)			
–O(54)	3.31(3)				

https://doi.org/10.1346/CCMN.1992.0400201 Published online by Cambridge University Press

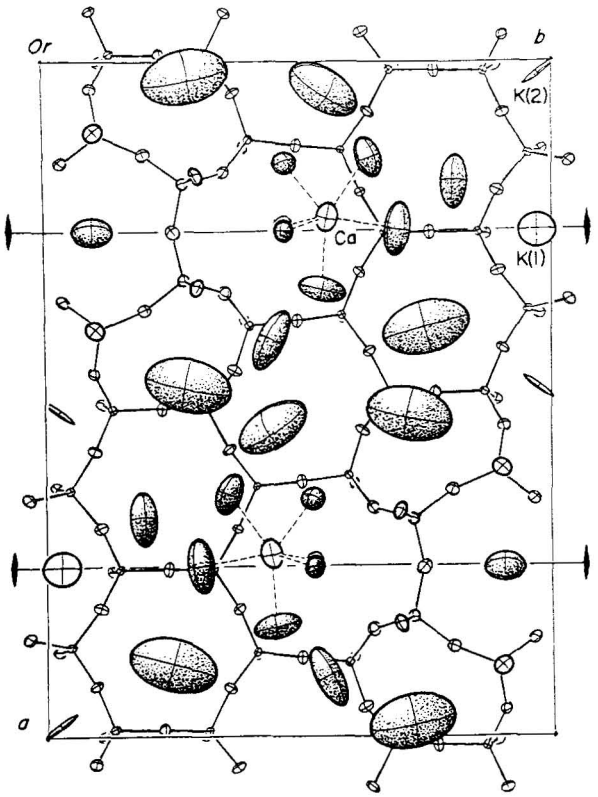

Figure 6. Projection of all interlayer species at $z = 0$ and the silicate sheet below (same as in Figure 2) with 50%-probability ellipsoids as determined for Broken Hill bannisterite. Water molecules are shaded. The crystallographic 2-fold axes are indicated.

of the adjacent silicate layer) are shown in Figure 6. These uncertainties are expressed also in abnormal distances involving these atoms. For example, the distance O(54)–O(56) is only 2.3 Å, but if this atom were placed on the electron density maximum (Figure 4) the distance would be 2.66 Å, and other contacts would also be more nearly normal. Such displacements are comparable to corresponding thermal vibrations.

When the occupancies of all the water molecules found in the interlayer region are summed the result is 3.2 molecular waters in the Broken Hill specimen, as compared with the analytical total of 5.1. Refinement of bannisterite from Franklin Furnace yielded 2.9 water molecules, considerably less than the 5.5 water species determined by Dunn *et al.* (1981). Because of the highly diffuse character of the water not associated with the calcium ion, it is not possible for our model to account for all the water in the interlayer region.

SUMMARY

Solution and refinement of the structures of two compositionally different bannisterites yielded virtually identical results. Trioctahedral mica-like layers are cross-linked via inverted tetrahedra, creating large interlayer regions containing Ca, K, and H_2O groups. The octahedral sheet has an undulant geometry along *b*, and bannisterite can properly be classified as a modulated layer silicate, as described by Guggenheim and Eggleton (1988). Al is concentrated into the inverted tetrahedra, and local variations in the Al/Si arrangement within these tetrahedra appear to induce positional disorder among the interlayer species. Finally, we suggest that bannisterite is best described by the idealized formula:

$$Ca_{0.5}K_{0.5}M_{10}[Si_{14.5}Al_{1.5}]O_{38}(OH)_8 \cdot nH_2O,$$

where M is the octahedrally-coordinated divalent cation (Fe, Mn, Zn, Mg), and n ranges from 2 to 6.

ACKNOWLEDGMENTS

The authors would like to acknowledge their debt to the late Ian Threadgold, whose early abstract on the structure of bannisterite served as an invaluable guide to this work. In addition, Stephen Guggenheim and S. W. Bailey offered timely encouragement and important advice. At the Smithsonian Institution, Daniel Appleman devoted a great amount of time towards the computer calculations required for this project, and George Guthrie provided his assistance in sample selection. Embaie Ferrow kindly shared his preliminary TEM results with us, and Pete Dunn offered eager discussion. L. W. Finger and E. E. Foord provided valuable criticism of the manuscript.

REFERENCES

Burnham, C. W. (1963) Refinement of the crystal structure of sillimanite: *Z. Kristalogr.* **118,** 127–148.

Dunn, P. J., Leavens, P. B., Norberg, J. A., and Ramik, R. A. (1981) Bannisterite: New chemical data and empirical formulae: *Amer. Mineral.* **66,** 1063–1067.

Eggleton, R. A. (1972) The crystal structure of stilpnomelane. Part II. The full cell: *Mineral. Mag.* **38,** 693–711.

Eggleton, R. A. and Guggenheim, S. (1986) A re-examination of the structure of ganophyllite: *Mineral. Mag.* **50,** 307–315.

Ferrow, E. A., Morad, S., Koark, H. J., and Ounchanum, P. (1990) Bannisterite from the Nyberget Mn-Fe ore deposits, central Sweden: *Geol. Soc. Amer. Abstr. Progr.* **22,** A261.

Foshag, W. F. (1936) Ganophyllite and zincian amphibole from Franklin Furnace, New Jersey: *Amer. Mineral.* **21,** 63–67.

Guggenheim, S. and Eggleton, R. A. (1986) Structural modulations in Mg-rich and Fe-rich minnesotaite: *Can. Mineral.* **20,** 479–497.

Guggenheim, S. and Eggleton, R. A. (1987) Modulated 2:1 layer silicates: Review, systematics, and predictions: *Amer. Mineral.* **72,** 724–738.

Guggenheim, S. and Eggleton, R. A. (1988) Crystal chemistry, classification, and identification of modulated layer silicates. *Reviews in Mineralogy* **19,** Mineral Soc. Amer., 675–725.

Ibers, J. A. and Hamilton, W. C. (1974) *International Tables*

for X-ray Crystallography: Vol. IV, Kynoch Press, Birmingham, England, 273–284.

Jones, J. B. (1968) Al–O and Si–O tetrahedral distances in aluminosilicate framework structures: *Acta Crystallogr.* **B24,** 355–358.

Karle, J. and Karle, I. L. (1966) The symbolic addition procedure for phase determination for centrosymmetric and noncentrosymmetric crystals: *Acta Crystallogr.* **B21,** 849–859.

Lopes-Vieira, A. and Zussman, J. (1969) Further detail on the crystal structure of zussmanite: *Mineral. Mag.* **37,** 49–60.

Matsubara, S. and Kato, A. (1989) A barian bannisterite from Japan: *Mineral. Mag.* **53,** 85–87.

Plimer, I. R. (1977) Bannisterite from Broken Hill, Australia: *Neues Jb. Mineral. Monatsh.* **11,** 504–508.

Smith, M. L. and Frondel, C. (1968) The related layered minerals ganophyllite, bannisterite, and stilpnomelane: *Mineral. Mag.* **36,** 893–913.

Smith, W. C. (1948) Ganophyllite from the Benallt mine, Rhiw, Caernarvonshire: *Mineral. Mag.* **28,** 343–352.

Stewart, J. M. and Hall, S. R. (1988) *The XTAL2.4 System of Crystallographic Programs:* University of Maryland and University of Western Australia, College Park, MD.

Thompson, J. B. (1978) Biopyroboles and polysomatic series: *Amer. Mineral.* **63,** 239–249.

Threadgold, I. (1979) Ferroan bannisterite—a new type of layer silicate structure: in *Abstract, Seminar on Broken Hill,* The Mineral. Soc. of New South Wales and the Mineral. Soc. of Victoria, Australia.

Zussman, J. (1954) Investigation of the crystal structure of antigorite: *Mineral. Mag.* **40,** 498–512.

(Received 22 July 1991; accepted 5 November 1991; Ms. 2120)